

Magnetodielectric effect and optic soft mode behaviour in quantum paraelectric EuTiO_3 ceramics

S. KAMBA¹, D. NUZHNYI¹, P. VANĚK¹, M. SAVINOV¹, K. KNÍŽEK¹, Z. SHEN², ŠANTAVÁ¹, K. MACA³, M. SADOWSKI⁴ and J. PETZELT¹

¹ *Institute of Physics ASCR, v.v.i. Na Slovance 2, 182 21 Prague 8, Czech Republic*

² *Arrhenius Laboratory, Stockholm University, SE-10691 Stockholm*

³ *Brno University of Technology, Technická 2896/2, 616 69 Brno, Czech Republic*

⁴ *Grenoble High Magnetic Field Lab, CNRS, 25, avenue des Martyrs, Grenoble Cedex 9, France*

PACS 75.80.+q – Magnetomechanical and magnetoelectric effects, magnetostriction

PACS 78.30.-j – Infrared and Raman spectra

PACS 63.20.-e – Phonons in crystal lattices

PACS 77.22.-d – Dielectric properties of solids and liquids

Abstract. - Infrared reflectivity and time-domain terahertz transmission spectra of EuTiO_3 ceramics revealed a polar optic phonon at 6 - 300 K whose softening is fully responsible for the recently observed quantum paraelectric behaviour. Even if our EuTiO_3 ceramics show lower permittivity than the single crystal due to a reduced density and/or small amount of secondary pyrochlore $\text{Eu}_2\text{Ti}_2\text{O}_7$ phase, we confirmed the magnetic field dependence of the permittivity, also slightly smaller than in single crystal. Attempt to reveal the soft phonon dependence on the magnetic field at low temperatures remained up to 13 T below the accuracy of our infrared reflectivity experiment.

Multiferroics exhibiting simultaneously ferroelectric and ferro- or antiferromagnetic order are known since the beginning of the 1960's, but the interest to these materials underwent a revival after the pioneering work by Wang et al. [1] who in the BiFeO_3 thin films revealed spontaneous polarization and magnetization almost by an order of magnitude higher compared to the bulk samples. Recently, much attention have been paid to the multiferroic materials not only because of their rich and fascinating fundamental physics (questions why only few materials with simultaneous ferroelectric and magnetic order are known, how to explain the coupling of magnetic and ferroelectric order etc.), but also because of the promising potential applications in multiple-state memory elements. [2, 3] In magnetoelectrics the polarization can be controlled by the magnetic field as well as the magnetization by the electric field and so magnetic field tuning of the dielectric permittivity ϵ' (magnetodielectric effect) is expected. Recently, gigantic proper magnetodielectric effect has been observed e. g. in TbMnO_3 [4] and EuTiO_3 . [5] Large magnetodielectric effect was recently seen also in BiFeO_3 [6], however in this case the change of ϵ' with magnetic field is not due to coupling of the polarization and magnetization, but due

to combination of inhomogeneous magnetoresistance and Maxwell-Wagner effect. [6]

The perovskite EuTiO_3 is not a typical multiferroic. It exhibits an antiferromagnetic (AFM) structure below $T_N = 5.3$ K, [7] but the ferroelectric order does not take place because the quantum fluctuations prevent the freezing of polarization at low temperatures. Its permittivity increases on cooling similarly to classical quantum paraelectrics [9, 10] (incipient ferroelectrics) SrTiO_3 , KTaO_3 , etc., but it saturates below ~ 30 K and sharply drops down at T_N . [5] Magnetic structure of EuTiO_3 was investigated already forty years ago [7] and determined in Ref. [8]. A neutron-diffraction study of a powder sample revealed the G type AFM structure. [7] In this magnetic arrangement, there are two interpenetrating *fcc* sublattices in which a given Eu^{2+} has six nearest-neighbor Eu^{2+} with antiparallel spins and 12 next-nearest-neighbor Eu^{2+} with parallel spins. At 1.3 K the magnetic moment increases linearly with magnetic field up to 1 T and above 1.4 T the moment saturates at 156 emu/g ($6.93 \mu_B$). [7]

The low-temperature ϵ' below T_N exhibits a huge dependence on the magnetic field B , giving evidence about a large interaction of magnetic moments with the crystal

lattice. [5] ϵ' strongly increases even for low B and the drop down in ϵ' seen near T_N at 0 T disappears at fields above 1 T so that only quantum paraelectric behaviour is seen at high magnetic fields down to 2 K. Katsufuji and Takagi [5] suggested that the temperature dependence of ϵ' is due to a soft optic phonon reducing its frequency on cooling and the decrease in ϵ' near T_N occurs due to the strong coupling of localized spins in the $4f$ levels of Eu^{2+} with the soft F_{1u} phonon. The transverse-field Ising model and Heisenberg model were successfully applied for explaining the dielectric and magnetic properties of EuTiO_3 and $\text{Eu}_{1-x}\text{Ba}_x\text{TiO}_3$ with and without external magnetic and electric fields. [11–15] Jiang and Wu [11] calculated the soft mode frequency and obtained 8 cm^{-1} at 20 K. Fennie and Rabe [16] calculated the soft mode frequency in the AFM phase from the first principles and obtained 77 cm^{-1} . They also predicted a remarkable softening of the soft mode and transition into the ferroelectric phase in biaxially strained samples. The strain can be realized in thin films deposited on substrates with slightly mismatched lattice parameters. [16] In such a phase the giant magnetodielectric effect is expected.

The polar soft mode is infrared (IR) active so that the IR spectroscopy is the best tool for the verification of the predicted phonon softening on cooling. In this letter we will show that the soft mode really exhibits the expected softening (from 112 cm^{-1} at 300 K to 82 cm^{-1} at 6 K), in perfect agreement with the predictions from the first-principles calculations. [16]

EuTiO_3 ceramics was synthesized from the Eu_2O_3 and Ti_2O_3 powders using mechanochemical activation in the planetary micromill Fritsch Pulverisette 7. Powder XRD showed strong amorphization - no diffraction line of Eu_2O_3 were found but significantly widened peaks of the Ti_2O_3 and of some unidentified phases. The powder was pressed into pellet in a uniaxial press at 650 MPa (or in an iso-static press at 300 MPa) at room temperature and then annealed at 1500°C in $\text{Ar} + 10\%\text{H}_2$ atmosphere. The reducing atmosphere is necessary to prevent the formation of pyrochlore $\text{Eu}_2^{3+}\text{Ti}_2^{4+}\text{O}_7$. The powder XRD showed sharp diffraction lines corresponding to single-phase cubic perovskite EuTiO_3 . No other phase was detected, but the porosity of resulting ceramics was relatively high - 20-30%. Therefore we used an additional sample processing: The EuTiO_3 pellet was ground and milled again to a fine nanopowder which was sintered by spark plasma sintering (temperature $1150\text{--}1200^\circ\text{C}$, pressure 75-100 MPa, time 3-5 min). The resulting ceramic samples were more than 91% dense and contained 5% or in one case even 15% of the secondary pyrochlore phase.

The magnetodielectric effect was studied by measuring the changes in permittivity with the magnetic fields up to 14 T (PPMS, Quantum design) at temperatures 2-300 K. The measurements were performed at frequency 1 kHz with ultra-precision capacitance bridge Andeen-Hagerling 2500A. Details of the dielectric, THz and IR experiments performed without magnetic field are described elsewhere.

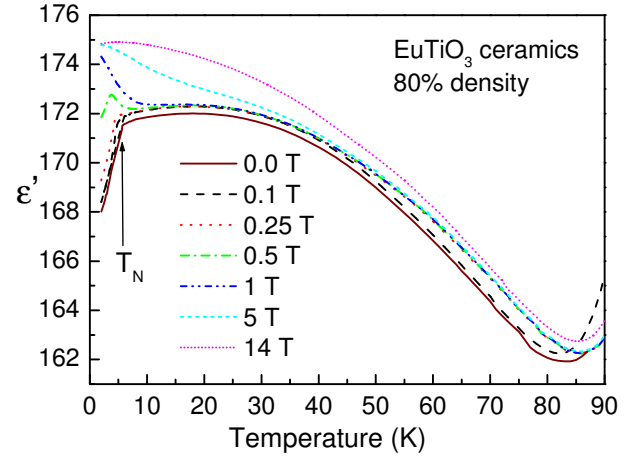


Fig. 1: (color online) Temperature dependence of the permittivity in EuTiO_3 ceramics measured at 1 kHz and at various magnetic fields. Critical temperature to AFM phase is marked.

[6] The IR reflectivity spectra were taken as well at magnetic fields up to 13 T at 1.8 K using a Fourier transform IR spectrometer Bruker IFS 113v.

Temperature dependence of ϵ' below 90 K measured at various magnetic fields is plotted in Fig. 1. At higher temperature the sample becomes slightly conducting, [17] therefore ϵ' increases to huge values (not shown in Fig. 1) due to Maxwell-Wagner polarization mechanism. Below 85 K, one can see an increase in intrinsic permittivity on cooling and its saturation below $\sim 25\text{ K}$ due to quantum fluctuations. The shape of the $\epsilon'(T)$ curve down to 6 K is the same as in classical quantum paraelectric SrTiO_3 , [9] but with much lower value. Sharp drop appears in $\epsilon'(T)$ below AFM phase transition at $T_N=5.3\text{ K}$, although the sample remains paraelectric. At high magnetic fields above 1 T the AFM phase transforms to the ferromagnetic one, drop down in $\epsilon'(T)$ disappears and a pure incipient ferroelectric behaviour, i.e. continuous increase of $\epsilon'(T)$ on cooling is seen. We note that the same temperature and magnetic field dependences of ϵ' were observed independently on orientation of magnetic \mathbf{B} and measuring electric \mathbf{E} fields (i.e. both geometries $\mathbf{E}\parallel\mathbf{B}$ and $\mathbf{E}\perp\mathbf{B}$ gave the same $\epsilon'(T, \mathbf{B})$ results as in Fig. 1). Similar $\epsilon'(T, \mathbf{B})$ was observed by Katsufuji and Takagi on EuTiO_3 single crystal, but the value of permittivity was more than twice higher compared with our values obtained on the ceramics of 80% density. This discrepancy could be due to the porosity which may cause a 50% decrease in the permittivity. [18]

ϵ' decreases with the AFM ordering of Eu spins whereas it increases with their ferromagnetic arrangement under magnetic field. Therefore Katsufuji and Takagi suggested that the $\epsilon'(\mathbf{B})$ is dominated by the pair correlation of the Eu neighbouring spins $\langle \mathbf{S}_i \cdot \mathbf{S}_j \rangle$ and successfully fitted the

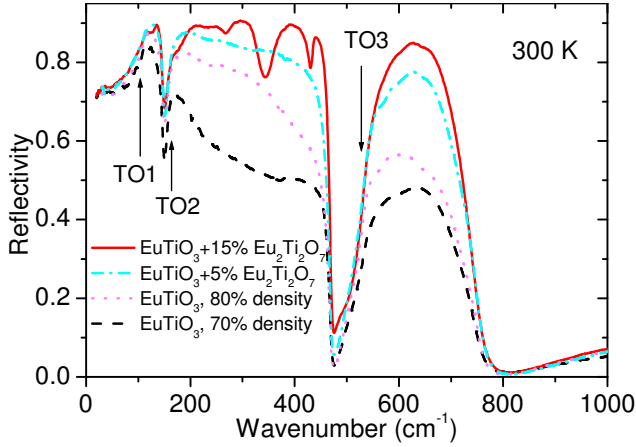


Fig. 2: (color online) Room-temperature IR reflectivity spectra of EuTiO_3 ceramics of 70 and 80 % density as well as $\text{EuTiO}_3 + 15\% \text{Eu}_2\text{Ti}_2\text{O}_7$ (93.6% density) and $\text{EuTiO}_3 + 5\% \text{Eu}_2\text{Ti}_2\text{O}_7$ (91% density). Transverse phonon frequencies of three perovskite modes are marked.

experimental $\varepsilon'(T)$ data by the formula

$$\varepsilon'(T, \mathbf{B}) = \varepsilon'_0(T)(1 + \alpha \langle \mathbf{S}_i \cdot \mathbf{S}_j \rangle), \quad (1)$$

where $\varepsilon'_0(T)$ is the dielectric constant in the absence of a spin correlation and α is the coupling constant between correlated spins and permittivity. The same authors also suggested that the value of static permittivity is only due to contributions of polar optic phonons and the temperature dependence of ε'_0 is caused by softening of one of the phonons, similarly as in SrTiO_3 . Our radio-frequency dielectric measurements without magnetic field really did not reveal any frequency dispersion in ε' and only negligible dielectric losses between 100 Hz and 1 MHz.

For confirmation of the anomalous polar phonon we performed THz transmission and IR reflectivity measurements between 6 and 300 K. IR spectra show strong dependence on the density of the ceramics as well as on the amount of pyrochlore $\text{Eu}_2\text{Ti}_2\text{O}_7$ secondary phase (see Fig. 2). Low-dense pure perovskite ceramics shows a large diffuse scattering, which rises with increasing frequency and deteriorates the IR reflectivity. 93.6% dense EuTiO_3 ceramics with 15% of $\text{Eu}_2\text{Ti}_2\text{O}_7$ secondary phase exhibits no diffuse scattering but additional reflection bands between 100 and 450 cm^{-1} , corresponding to polar phonons of the pyrochlore phase, while in the perovskite cubic phase only 3 IR active phonons are allowed. As an optimal compromise we decided to present here the low-temperature spectra of the sample with 5% of pyrochlore phase (91% density) which exhibits only weak diffuse scattering and the bands from pyrochlore phase are also very weak (see Figs. 2 and 3).

Fig. 3 shows corresponding IR reflectivity spectra at selected temperatures. One can see an increase of reflectivity on cooling due to the reduced phonon damping at low temperatures, as well as the shift of the first reflection

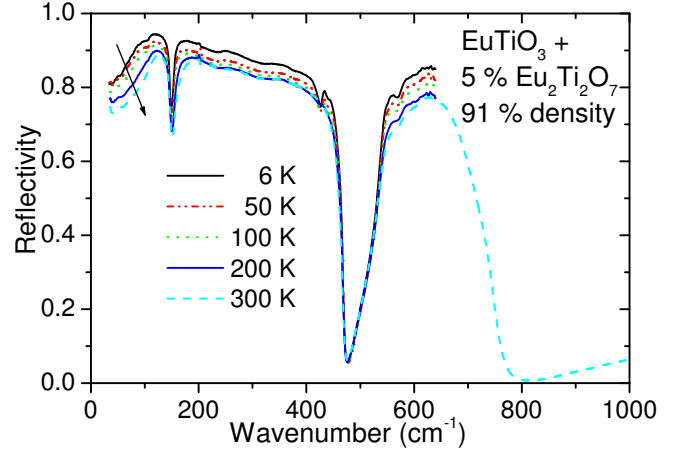


Fig. 3: (color online) IR reflectivity spectra of the EuTiO_3 ceramics at various temperatures. Increase in temperature is marked by the arrow. Softening of the low-frequency phonon on cooling is clearly seen. Note that $1 \text{ cm}^{-1} = 30 \text{ GHz}$.

band (i.e. the soft mode) to lower frequencies on reducing temperature. Complex permittivity $\varepsilon^*(\omega)$ is related to the reflectivity $R(\omega)$ by

$$R(\omega) = \left| \frac{\sqrt{\varepsilon^*(\omega)} - 1}{\sqrt{\varepsilon^*(\omega)} + 1} \right|^2. \quad (2)$$

For the fit of the IR and THz spectra we used a generalized-oscillator model with the factorized form of the complex permittivity:

$$\varepsilon^*(\omega) = \varepsilon_\infty \prod_j \frac{\omega_{LOj}^2 - \omega^2 + i\omega\gamma_{LOj}}{\omega_{TOj}^2 - \omega^2 + i\omega\gamma_{TOj}} \quad (3)$$

where ω_{TOj} and ω_{LOj} denotes the transverse and longitudinal frequency of the j -th polar phonon, respectively, and γ_{TOj} and γ_{LOj} denotes their corresponding damping constants. The high-frequency permittivity ε_∞ resulting from the electron absorption processes was obtained from the room-temperature frequency-independent reflectivity tails above the phonon frequencies and was assumed temperature independent.

Real and imaginary parts of $\varepsilon^*(\omega)$ obtained from the fits to IR reflectivity are shown together with the experimental THz spectra in Fig. 4. One can clearly see the increase in static permittivity on cooling (zero frequency values in Fig. 4a) due to the softening of the two lowest frequency phonons. The maxima in $\varepsilon''(\omega)$ correspond roughly to the phonon eigen-frequencies.

EuTiO_3 crystallizes in the cubic $Pm\bar{3}m$ structure, which allows $3F_{1u}$ IR active phonons and no Raman active mode. Our Raman spectra really revealed no first order peak. In IR spectra we see three distinct reflection bands corresponding to phonon frequencies at 82, 153 and 539 cm^{-1} (at 6 K), however the fits were performed on the whole with 12 (mostly weak) modes,

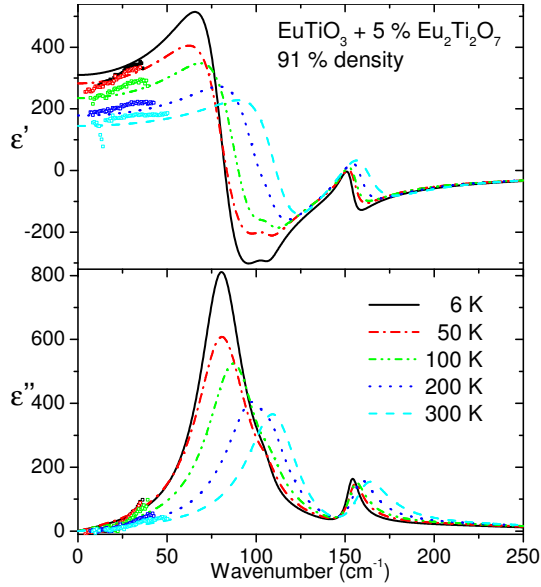


Fig. 4: (color online) Complex dielectric spectra of EuTiO₃ ceramics obtained from the fits of the IR reflectivity at selected temperatures. Spectra above 250 cm⁻¹ are not plotted since they show negligible temperature dependence. Dots correspond to the data evaluated from the THz spectra.

which account for the small rippled shape of reflectivity (mostly between 100 and 450 cm⁻¹). The additional peaks stem apparently from the secondary pyrochlore Eu₂Ti₂O₇ phase since they are better resolved in the sample with 15% pyrochlore phase (Fig. 2). We studied also temperature dependence of IR reflectivity of the 80%-dense single phase perovskite sample used for the magnetodielectric experiment in Fig. 1. The spectra yield the *same temperature dependence of the soft mode*, however, we do not present the spectra because of the deteriorated reflectance above 200 cm⁻¹.

In Fig. 5 the temperature dependence of the soft mode frequency ω_{SM} is plotted together with its dielectric strength $\Delta\epsilon_{SM}$. The soft mode softens from 112 cm⁻¹ (300 K) down to 82 cm⁻¹ (6 K) and therefore also the $\Delta\epsilon_{SM}$ increases. The low-temperature value of ω_{SM} reasonably corresponds to the soft mode frequency obtained from the first principle calculations by Fennie and Rabe, [16], but is one order of magnitude larger than the value estimated by Jiang and Wu [11]. In classical paraelectrics above the ferroelectric phase transition T_C , the ω_{SM} should obey the Cochran law $\omega_{SM} = \sqrt{A(T - T_C)}$. Our fit in Fig. 5 yields $A = 20.3 \text{ cm}^{-2} \text{ K}^{-1}$ and $T_C = -298 \text{ K}$. However, the fit is of low quality since the experimental ω_{SM} saturates at low temperatures below 50 K. Therefore it is more justified to use the Barrett formula [19]

$$\omega_{SM}(T) = \sqrt{A \left[\left(\frac{T_1}{2} \right) \coth \left(\frac{T_1}{2T} \right) - T_0 \right]}, \quad (4)$$

which takes into account the quantum fluctuation at low

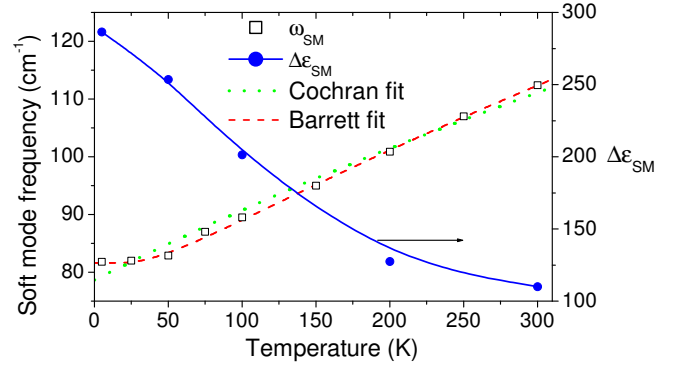


Fig. 5: (color online) Temperature dependence of the soft mode frequency fitted with Cochran and Barrett formula. The right scale shows the temperature dependence of the soft mode contribution to the static ϵ'

temperatures. The fit with Eq. 4, which is much more accurate especially at low temperatures (see Fig. 5), yields the following parameters: $A = 24.4 \text{ cm}^{-2} \text{ K}^{-1}$, $T_0 = -213 \text{ K}$ and $T_1 = 119 \text{ K}$. T_1 is the temperature below which the quantum fluctuations start to play a role ($\frac{1}{2}k_B T_1$ is the zero-point vibration energy) and T_0 is the critical temperature, which in our case is negative indicating the tendency to hypothetical lattice instability at negative temperatures.

Up to now discussed IR and THz spectra were taken above 6 K, i.e. above T_N . Since the permittivity decreases below T_N , we may expect an increase in ω_{SM} in the AFM phase and its softening on applied magnetic field. In a different setup we therefore measured the IR reflectivity from 30 to 300 cm⁻¹ at 1.8 K in the magnetic field from 0 to 13 T. Unfortunately, due to the low IR signal and limited accuracy of the measurement, we could not observe any reliable magnetic field dependence of our FIR reflectivity. The expected change of ω_{SM} with the highest magnetic field is only 3 cm⁻¹, which lies below limit of accuracy of the IR experiment using the magnetic cryostat.

Finally we conclude that our IR experiment confirmed the predictions of Refs. [5] that the quantum paraelectric behaviour in EuTiO₃ is caused by a soft optic phonon and its frequency corresponds to value calculated from the first principles. [16] However, the expected change of ω_{SM} with magnetic field was not detected due to the low accuracy of IR reflectivity measurements in the magnetic cryostat. The effect is expected to be larger in a single crystal or strained thin films, which will be subject of our next studies.

The work was supported by the Grant Agency of the Czech Republic (Project No. 202/06/0403), AVOZ10100520, Ministry of Education (OC101 and OC102-COST539) and European grant RITA-CT-2003-505474. The authors are grateful to V. Studnička for the

XRD analysis.

REFERENCES

- [1] J. Wang et al. *Science*, **299** (2003) 1719.
- [2] M. Fiebig, *J. Phys. D: Appl. Phys.*, **38** (2005) R123 .
- [3] S.-W. Cheong and M. Mostovoy, *Nature Mater.*, **6** (2007) 13.
- [4] T. Kimura, T. Goto, H. Shintani, K. Ishizaka, T. Arima and Y. Tokura, *Nature*, **426** (2003) 55.
- [5] T. Katsufuji and H. Takagi, *Phys. Rev. B*, **64** (2001) 054415.
- [6] S. Kamba et al. *Phys. Rev. B*, **75** (2007) 024403.
- [7] T.R. McGuire et al. *J. Appl. Phys.* **37** (1966) 981.
- [8] Ch.-L. Chien, S. DeBenedetti, and F. De S. Barros, *Phys. Rev. B*, **10** (1974) 3913.
- [9] K.A. Müller and H. Burkard, *Phys. Rev. B* **19** (1979) 3593.
- [10] G. A. Samara, *Solid State Physics, Advances in Research and Applications*, Vol. 56. San Diego: Academic Press, pp. 240-458 (2001) and references therein.
- [11] Q. Jiang and H. Wu, *J. Appl. Phys.*, **93** (2003) 2121.
- [12] S.J. Gong and Q. Jiang, *Phys. Stat. Sol. (b)*, **241** (2004) 3033.
- [13] H. Wu, Q. Jiang and W.Z. Shen, *Phys. Lett. A*, **330** (2004) 358.
- [14] H. Wu, Q. Jiang and W.Z. Shen, *Phys. Rev. B*, **69** (2004) 014104.
- [15] H. Wu and W.Z. Shen, *Sol. State Commun.*, **133** (2005) 487.
- [16] C.J. Fennie and K. M. Rabe, *Phys. Rev. Lett.*, **97** (2006) 267602.
- [17] T. Katsufuji and Y. Tokura, *Phys. Rev. B* **60** (1999) R15021.
- [18] I. Rychetský, J. Petzelt, T. Ostapchuk, *Appl. Phys. Lett.*, **81** (2002) 4224.
- [19] Y. Minaki et al. *J. Korean Phys. Soc.*, **42** (2003) S1290.